Available online at www.sciencedirect.com
ScienceDirect
Journal of Power Sources 175 (2008) 317–324
JOURNAL OF POWER SOURCES
www.elsevier.com/locate/jpowsour

Electrochemical oxidation of borohydride at nano-gold-based electrodes: Application in direct borohydride fuel cells

Fazlil A. Coowar [a,*], Girts Vitins [a], Gary O. Mepsted [a], Susan C. Waring [b], Jacqueline A. Horsfall [b]

[a] *QinetiQ, Haslar Marine Technology Park, Gosport, Hampshire PO12 2AG, UK*
[b] *Department of Materials and Applied Science, Cranfield University, Shrivenham, Swindon, Oxfordshire SN6 8LA, UK*

Received 29 June 2007; received in revised form 24 August 2007; accepted 16 September 2007
Available online 29 September 2007

Abstract

Nano-particulate gold-based materials along with commercial gold supported over carbon were investigated as possible alternative electrocatalysts for the oxidation of borohydride in alkaline media. Cyclic voltammetry experiments conducted on these materials show very high activity for the nano-particulate materials compared to the commercial materials despite a lower loading of gold (0.8 mg cm^{-2} compared to 1.0 mg cm^{-2}) and lower interface area in the nano-particulate materials. The presence of BH_4^- appears to have detrimental effect on the performances of the air-electrode for oxygen reduction. The current density recorded at −0.6 V versus Hg/HgO has decreased by a factor of six for silver nitrate AC65 while for MnO_2 a reduction in the current density by a factor of two only was observed. The implementation of the nano-particulate gold-based materials and the air-electrodes along with a low-cost anionic membrane in QinetiQ's tubular cell design has led to power density exceeding 28 mW cm^{-2} obtained at ambient temperature.

Keywords: Electrocatalysts; Borohydride tubular fuel cells; Nano-materials; Anionic membrane

1. Introduction

Proton exchange membrane electrolyte fuel cells (PEMFCs) based on hydrogen as a fuel have advanced substantially but their successful commercialisation is restricted by safety and storage efficiency of this flammable gas [1–4]. Therefore, certain liquid-fuels, such as methanol, ethanol, propanol, ethylene glycol, and diethyl ether, have been considered for fuelling PEMFCs directly [5]. Among these, methanol, with a theoretical capacity of 5.06 Ah g^{-1} and a hydrogen content of 12.8 wt%, is unambiguously the most attractive organic liquid-fuel at present for directly fuelled PEMFCs. Such fuel cells are referred to as direct methanol fuel cells, DMFCs [6–8]. The low cell voltage and power density due to poisoning of the anode during methanol oxidation and the phenomenon of methanol crossover limits the application of direct methanol fuel cells (DMFCs). One solution to this problem is to explore other promising hydrogen-carrying liquid-fuels, such as sodium borohydride, because of its high energy density and high cell.

$NaBH_4$ oxidises in strong alkaline media at pH greater than 12, to BO_2^- and water, and generates eight electrons

$$BH_4^- + 8OH^- \rightarrow BO_2^- + 6H_2O + 8e^- \quad (E_0 = -1.24\,V) \tag{1}$$

With the oxidation of $NaBH_4$ at the anode, the atmospheric oxygen is electrochemically reduced at the interface between the cathode catalyst and the aqueous electrolyte, and the electrons are consumed

$$2O_2 + 4H_2O + 8e^- \rightarrow 8OH^- \quad (E_0 = 0.40\,V) \text{ for } p(OH) = 0 \text{ or } pH = 14 \tag{2}$$

The coupling of reaction (1) with reaction (2) leads to an overall reaction (3) that is independent of pH.

$$BH_4^- + 2O_2 \rightarrow BO_2^- + 2H_2O \quad (E_{Cell} = 1.64\,V) \tag{3}$$

* Corresponding author. Tel.: +44 23 9233 5443; fax: +44 23 9233 5102.
E-mail address: facoowar@qinetiq.com (F.A. Coowar).

0378-7753/$ – see front matter © 2007 Elsevier B.V. All rights reserved.
doi:10.1016/j.jpowsour.2007.09.063

The theoretical cell voltage is 1.64 V, 0.4 V higher than that of the PEMFC, and the specific capacity and energy density of $NaBH_4$ can reach 5.67 Ah g^{-1} and 9296 Wh kg^{-1}, respectively. Despite a higher theoretical voltage and faster anodic electro-oxidation rate [9,10] compared to DMFC, two main obstacles, BH_4^- crossover and the poor anodic efficiency of BH_4^- remain to be overcome for energy to be maximised.

The aim of this paper is to report on work to minimise side reactions taking place in a direct borohydride fuel cell through a judicious choice of its different components. To mitigate the chemical hydrolysis of the BH_4^-, for the anode nano-particulate gold-based materials were selected and fabricated as they were reported to be excellent electrocatalysts for borohydride oxidation and poor catalysts for its hydrolysis [9,11,12]. Commercial gold supported on carbon has been evaluated as anode electrocatalyst and its performance compared with QinetiQ's nano-particulate gold-based materials.

As for the cathode, commercially available air-electrodes as well as composite MnO_2-based electrodes were explored as the latter was reported to have considerable electrocatalytic activity for oxygen reduction in alkaline medium in presence of BH_4^- [13]. Membrane electrode assembly (MEA) using the best cathode and anode along with low-cost anionic membrane was fabricated, implemented in QinetiQ's tubular fuel cell design and evaluated at ambient temperature.

2. Experimental

2.1. Fabrication of composite anode Au/C on carbon cloth or Ni grid

The sodium borohydride oxidation electrocatalyst was gold dispersed over carbon. This supported material was purchased from E-Tek (USA) and consists of 20 wt% of metal loading on carbon Vulcan XC 72 (with a total surface area of ca. 250 $m^2\,g^{-1}$). The composite anode was fabricated by weighing appropriate amounts of catalyst and PTFE binder (60 wt% suspension in water from Aldrich) so that the final composite anode consisted of 90 wt% of supported catalyst and 10 wt% PTFE. Deionised water was added to the mixture and the overall mix was sonicated for 10 min. The resulting ink was then pasted onto a carbon cloth from Toray (Japan). After evaporation of the solvent, a composite anode with a loading 1.8–2.0 mg cm^{-2} of gold was obtained. For three-electrode type experiments, a more rigid Au/C electrode was prepared by rolling the composite film on Ni grid (Advent, UK).

2.2. Electrodeposited nano-particulate Au on nickel grid

The fabrication of nano-particulate gold onto gold-plated nickel grid was carried out at constant potential of −0.61 V versus saturated calomel electrode (SCE) in $HAuCl_4$-based electrolyte for a plating time of 5–10 min. The gold loading was estimated by measuring carefully the weight of the nickel grid substrate before and after electrodeposition and was ≤0.8 mg cm^{-2}. The nano-particulate gold appears as black deposit due to its fine porous morphology as opposed to golden colour for flat gold.

2.3. Electrodeposited nanobimetallic gold–platinum Au–Pt

The electrolyte used in this case was an aqueous solution of $H_2PtCl_6{\cdot}H_2O$ and $HAuCl_4$. The formation of nanobimetallic Au–Pt material was obtained by applying two different potential pulses for different length of time.

2.4. Characterisation of nano-particulate gold-based materials by SEM and EDAX

The samples were examined using a JSM 6500F field emission microscope at 15 kV accelerating voltage for SEM imaging. The samples were mounted onto the SEM stubs using colloidal graphite, with no sample preparation. The composition of samples was determined by EDAX using an accelerating voltage of 20 kV.

2.5. Conductivity measurements on anionic membranes

Anionic membranes (AM) of thickness 70 μm supplied by University of Cranfield, UK, were activated through a first immersion for 1 h in deionised water followed by a second immersion for 10 min in 0.1 M NaOH at 90 °C. After activation, they were left in 0.1 M NaOH at room temperature. The conductivity of membranes was tested at different time intervals after dipping in both 5 wt% $NaBH_4$ in 6 M NaOH. AC impedance spectroscopy was used to measure conductivity of the membrane using a two-electrode cell configuration with stainless steel as the current collector. Tests were performed by clamping membranes between two current collectors of 1.5 cm^2 area. The membranes were cut to size and soaked in 6 M NaOH. They were dabbed with paper prior to testing. Impedance analysis was performed using Solartron FRA 1260 + ECI 1287 system.

Conductivity measurements are summarised in Table 1. Ionic conductivity was measured at ambient temperature both in 6 M NaOH and in 5 wt% $NaBH_4$ in 6 M NaOH. High conductivity of 1.9×10^{-2} S cm^{-1} with good stability was obtained in 6 M NaOH. However, in presence of fuel, conductivity decreases dramatically and reaches conductivity value of 0.86 mS cm^{-1}. However, as shown in Table 1, the conductivity of this membrane does not deteriorate with time after more than 100 days in 5 wt% $NaBH_4$ in 6 M NaOH.

Table 1
Conductivity of the anionic membrane in 6 M NaOH and 5 wt% $NaBH_4$ in 6 M NaOH

Immersion time (days)	Conductivity in 6 M NaOH (mS cm^{-1})	Conductivity in 5 wt% $NaBH_4$ in 6 M NaOH (mS cm^{-1})
3	19	0.88
4	19	0.82
100	19	0.86

2.6. Air-electrodes

Three air-electrodes denoted AC65 (from Alu-Power/Yardney (USA)), E4 (from the Electric Fuel (Israel)) and γ-MnO_2 (Tosoh (Japan)) were used. All these composite electrodes contained carbon black as conductive additive and PTFE as the binder. AC65 and E4 were respectively silver nitrate ($AgNO_3$) and manganese-based catalysts supported on carbon black built on one side of the nickel grid. On the other side of the nickel grid, the gas diffusion layer made of carbon black and microporous PTFE film was attached to the supporting Ni grid.

For the home-made composite MnO_2 air-electrode, appropriate amounts of MnO_2, Vulcan XC72 and dry PTFE powder in a ratio of 20, 65 and 15 wt% were weighed. The mixture was thoroughly ground using mortar and pestle and rolled onto a nickel grid. In a similar way, a gas diffusion layer comprising of 60 wt% of Super P and 40 wt% of PTFE was prepared and transferred on the other side of the nickel grid. Finally, a microporous PTFE film from Goodfellow (UK) was attached to the carbon side of the electrode. To attain wet-proof property the air-electrode was treated in Ar at 300 °C for 1 h.

2.7. Electrochemical testing

The electrocatalytic activity of both cathode and anode was examined in a three-electrode cell set-up (Fig. 1) which consists of a reference electrode (RE) Hg/HgO in 6 M NaOH, a gold mesh counter electrode (CE) and the variable air-electrode or gold-based anode as the working electrode (WE); indeed using platinum as counter electrode would have resulted in harsh borohydride hydrolysis.

In order to avoid reducing the Hg/HgO reference electrode in the BH_4^- solution, the reference electrode was wrapped with a pre-treated Nafion membrane, which is impermeable to BH_4^-. The Nafion membrane was pre-treated by first boiling in 3 wt% of hydrogen peroxide H_2O_2 followed by a subsequent boiling for another hour in deionised water.

Cyclic voltammetry experiments at a rate of 5 mV s^{-1} were conducted in an electrolyte solution of 6 M NaOH under continuous flux of oxygen in the absence and presence of $NaBH_4$. The stability of the air-electrodes was gauged using chronocoulometry.

All the electrochemical testing of these catalysts was performed using a versatile multipotentiostat VMP3 (Bio-Logic, France). The geometrical area of the working electrode was 1 cm^2 with the catalyst coated on one side in the air-electrode testing (Fig. 1). Fig. 1 also shows the air-electrode with the electrocatalyst layer contacting the electrolyte solution and the hydrophobic gas diffusion layer exposing to air.

The anode materials (e.g. nano-particulate gold) prepared on grid had an electrode footprint of 1 cm^2 corresponding to ca. 2.56 cm^2 geometric surface. The sweep rate used was 5 mV s^{-1}. All the electrode potentials are given with respect to the Hg/HgO reference electrode unless stated otherwise.

2.8. Double-layer capacitance measurements

To assess interfacial area of different electrode interfaces, double-layer capacitance measurements were performed using the impedance set-up used for conductivity measurements in a frequency range from 0.1 Hz to 100 kHz, with a logarithmic distribution of 10 points per decade and an alternated signal of 10 mV amplitude. These measurements were carried out at open circuit voltage (OCV).

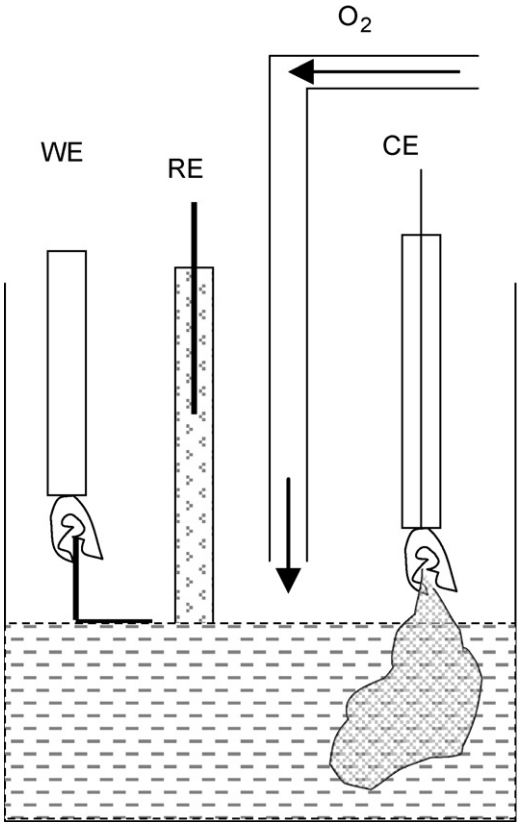

Fig. 1. Three-electrode set-up for oxygen reduction electrode testing.

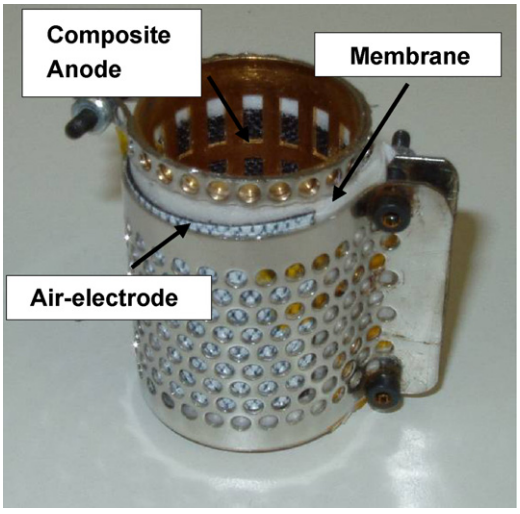

Fig. 2. QinetiQ's tubular fuel cell design.

2.9. Fabrication and testing of complete fuel cells

Fuel cells were assembled using QinetiQ's tubular cell design (Fig. 2) that consists of a perforated stainless steel tube. There was no preliminary hot-pressing procedure to prepare the membrane electrode assembly (MEA) as in other types of fuel cells, like PEMFC. Instead, the anode, membrane and cathode were placed around the hollow cylinder and clamped by a stainless steel grid, which provides good electrode/membrane interface. The electrode footprint area was 13 cm^2. The electrolyte with the fuel (i.e. 5 wt% of $NaBH_4$ in 6 M NaOH) was then added to the cylinder. Electrochemical tests were performed on a single cell by polarising from open circuit potential to 0.1 V by stepping down the potential in steps of 50 mV. The electrochemical testing of the cells was performed using the versatile multipotentiostat VMP3 (Bio-Logic, France) or using an Arbin battery tester. All the experiments were carried out at room temperature.

3. Results and discussion

3.1. Characterisation of nano-particulate materials by SEM

Fig. 3a and b shows respectively the SEM pictures of nano-particulate gold and nano-particulate bimetallic Au–Pt deposited onto gold-plated nickel grid. The SEM picture of nano-particulate gold shows agglomeration of gold particles the size of which is around 100 nm, as evidenced by Fig. 3a. Wide voids between clusters of gold particulates are clearly seen which provide channels for ionic transport. As shown in Fig. 3b, the SEM picture of the bimetallic Au–Pt material reveals a similar morphology to that of nano-gold, the particle size of which is around 100 nm. The deposit is highly porous probably of high surface area, which should favour ionic transport as in the case of nano-particulate gold. The composition of bimetallic Au–Pt material as determined by EDAX was 89 wt% of Au and 11 wt% of Pt.

3.2. Evaluation of electrocatalysts for borohydride oxidation

Fig. 4a shows the oxidation of BH_4^- ion at different electrode surfaces, commercial Au/C from E-Tek supported on gold-plated nickel grid, nano-particulate Au and nano-particulate bimetallic Au–Pt, both electroplated on gold-plated nickel grid and gold foil. Starting from a potential of around −1.1 V versus Hg/HgO and sweeping towards more positive values, the current density observed in the cyclic voltammogram at these four electrodes increases with increasing potential. A broad peak was observed at the nano-particulate gold electrode, which disappeared when the scan was reversed. However, no peak was found at nano-particulate bimetallic Au–Pt electrode, the commercial

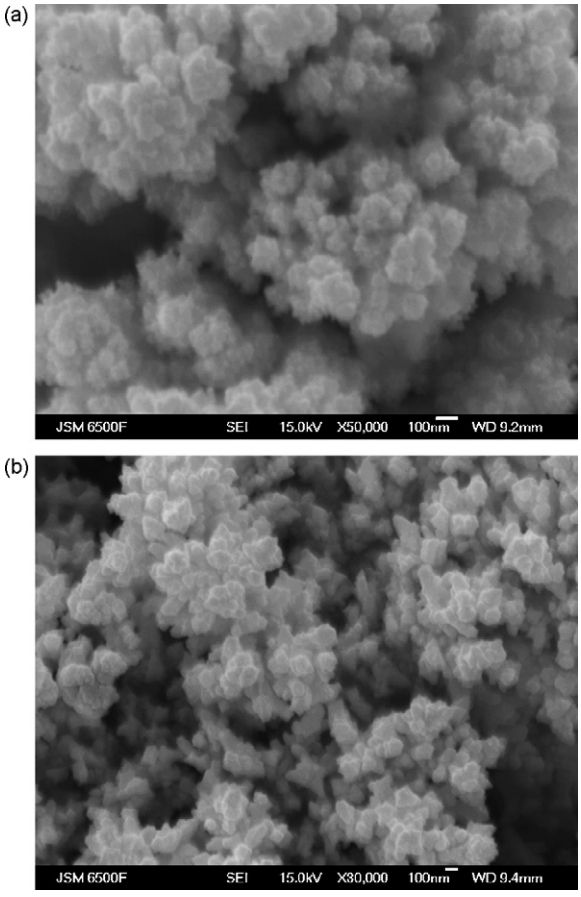

Fig. 3. SEM images of nano-Au (a) and nano-Au–Pt (b) anode materials.

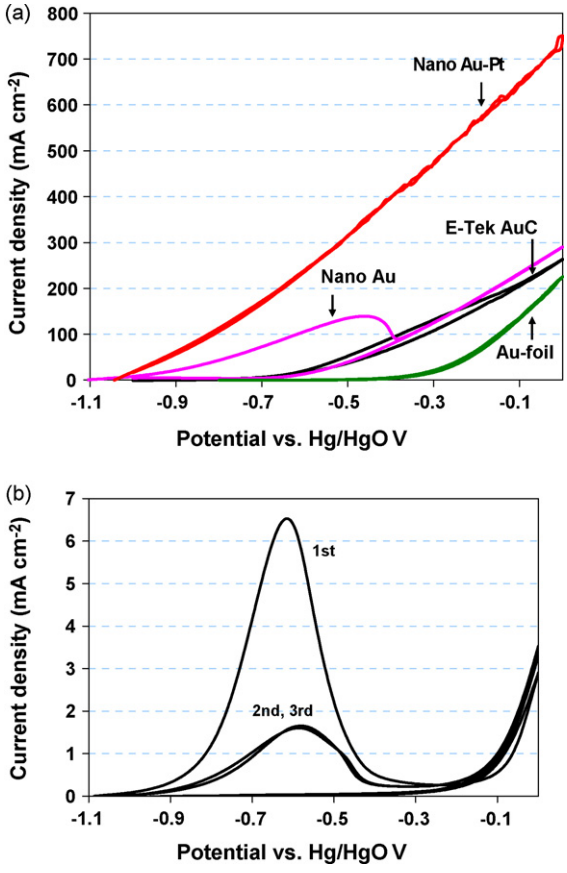

Fig. 4. Cyclic voltammetry of different anode materials (a) and the nickel grid substrate (b) in 5 wt% $NaBH_4$ in 6 M NaOH. Sweep rate 5 mV s^{-1}.

Table 2
Double-layer capacitance of different anode materials measured by AC impedance

Materials	Double-layer capacitance (F)	Geometric surface area (cm^2)	Surface enhancement	Catalyst loading ($mg\,cm^{-2}$)
Flat Au	5.2×10^{-5}	1.0	N/A	N/A
Nano-Au	1.6×10^{-3}	2.56	12	≤0.8
Nano-Au–Pt	5×10^{-3}	2.56	40	≤1.0
Au/C	0.12	3.2	Ca. 770	1.0

The catalyst loading is given per 1 cm^2 of footprint

Au/C electrode and the flat Au-foil electrode. It has to be pointed out that voltammograms were also recorded at all the electrocatalysts explored in an electrolyte solution of 6 M NaOH free of fuel. The open circuit voltages of these electrode materials were more positive in the fuel free 6 M NaOH and no significant current was recorded in the voltage range of interest. It is worth noting that the current density measured at the Au-foil electrode between the voltage range of −1 to −0.45 V is negligible and increases only after potential more positive than −0.3 V.

The onset of borohydride oxidation at the nano-particulate gold starts at a very negative potential −1.12 V probably caused by the oxidation of BH_3OH^- according to the following reaction:

$$BH_4^- + H_2O \rightarrow BH_3OH^- + H_2 \quad (4)$$

In fact, the open circuit voltage of the nano-particulate gold was −1.124 V, which could not be linked to H_2 oxidation since the equilibrium potential $E^{eq}(H^+/H_2)$ is equal to −0.928 V in sodium hydroxide solution [13]. Furthermore, the very low potential at which oxidation is observed can only be related to the BH_3OH^- oxidation, which was reported to occur around 0.5 V lower than that of BH_4^- on gold [14]. The absence of any peak at nano-particulate bimetallic Au–Pt, commercial Au/C and gold electrodes suggests that the tetrahydroborate oxidation mechanism at these electrodes is different. It is possible that the tetrahydroborate oxidation mechanism is influenced not only by the nature of electrocatalysts used but also by the nature of the supporting substrate.

The most striking features lie in the current delivered by the nano-particulate materials. For the nano-particulate gold electrode, on the forward scan, the current density measured from open circuit potential to −0.35 V is higher than the commercial Au/C electrode. For instance, at −0.8 V the current density is 50 times higher. For the nano-particulate Au–Pt electrode, regardless of the direction of the sweep, the current density is even higher than the nano-particulate gold over the whole potential range explored. At −0.8 V, the current density delivered by the nano-particulate bimetallic Au–Pt and the nano-particulate gold is respectively 100 times and 50 times greater than the commercial Au/C electrodes. To ensure that the current originates from the oxidation of borohydride or borohydride derivatives at these electrode surfaces and not from the nickel substrate, a control experiment was conducted at the nickel substrate.

Fig. 4b shows the voltammogram obtained at the latter electrode surface in 5 wt% $NaBH_4$ in 6 M NaOH. As shown in Fig. 4b, on the first scan, an anodic peak centred at −0.6 V with a current density of 6.5 $mA\,cm^{-2}$ is observed but disappeared upon reversal of potential. The intensity of this peak decreases with increasing number of cycles suggesting that this material is not active for oxidation of borohydride. The improved performances exhibited by the nano-particulate materials over flat gold could be explained by their large interfacial area. Double-layer capacitance measurement by AC impedance conducted in 6 M NaOH reveals a surface enhancement of 12 times for the nano-particulate gold and 40 times for the nano-particulate bimetallic Au–Pt compared to flat gold as summarised in Table 2.

A closer examination of Table 2 reveals a higher interfacial area for the commercial Au/C electrode with a surface enhancement much higher than the nano-particulate materials. It has to be noted that the high surface area carbon contributes to the high double-layer capacitance. As a result, higher electrocatalytic activity compared to the nano-particulate materials should be observed at this electrode. In addition, it has to be noted that the catalyst loading was 1.0 $mg\,cm^{-2}$ compared to 0.8 $mg\,cm^{-2}$ for the nano-particulate materials. However, this was found not to be the case as shown in Fig. 4a where the nano-particulate bimetallic gold–platinum showed higher current density over the entire voltage window investigated. It is possible that in this electrode the density of active sites is reduced due to the agglomeration of gold particles supported on the carbon surface.

The higher current density obtained with nano-particulate Au–Pt over the nano-particulate Au could be explained by the activity of gold for borohydride oxidation combined with the activity of platinum for both borohydride and hydrogen oxidation. These materials are two-component-based catalyst, one component to convert the borohydride to hydrogen and a second to oxidise hydrogen efficiently. In fact, Amendola et al. [9] have described studies of borohydride oxidation on high surface area electrodes, where the catalyst was gold or gold (97 wt%)–platinum (3 wt%) alloy. They have shown that the oxidation of borohydride occurs with a total number of electron exchange of ≈7 with moderate current densities at room temperatures, and current densities above 0.1 $A\,cm^{-2}$ at 70 °C.

3.3. Evaluation of electrocatalysts for oxygen reduction in 6 M NaOH and 5 wt% $NaBH_4$ in 6 M NaOH

Oxygen reduction was first investigated in oxygenated 6 M NaOH at three different electrode surfaces; two commercially available electrodes, E4, which is a manganese-based electrode from Electric Fuel Ltd. (Israel) and AC65, a silver-based

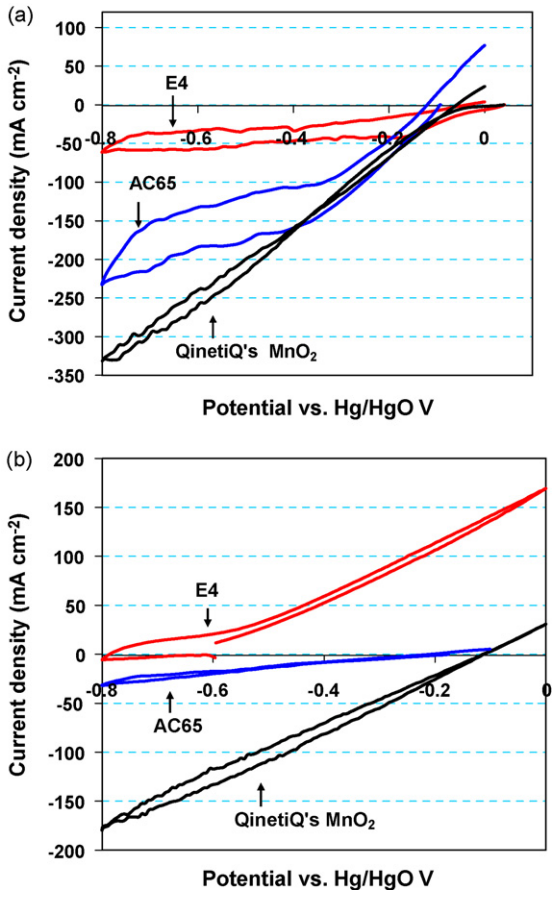

Fig. 5. Cyclic voltammograms of cathode materials in 6 M NaOH (a) and in 5 wt% $NaBH_4$ (b) under O_2 flux.

electrode, from Alupower/Yardney (USA) and a home-made composite electrode based on MnO_2. The OCVs of the manganese-based materials E4 and MnO_2-based electrode were more positive than AC65. The highest electrocatalytic activity was obtained with MnO_2 followed by AC65 and E4 (see Fig. 5a).

The same experiments were carried out in 5 wt% $NaBH_4$ in 6 M NaOH (see Fig. 5b). The open circuit potential of E4 electrode drops to around −0.6 V after 1 h immersion in oxygenated 5 wt% $NaBH_4$ in 6 M NaOH, which makes it unsuitable to be used as cathode material. However, the OCV of MnO_2 decreases at first and stabilises to an OCV of −0.116 V for more than 1 h in oxygenated 5 wt% $NaBH_4$ in 6 M NaOH while AC65 shows an OCV of around −0.190 V for the same length of time in the same solution. These differences in OCVs may be explained by the nature of the catalyst particles towards water management ability [15]. Despite E4 being a manganese-based catalyst, it is possible that it is more prone to be flooded by borohydride than MnO_2 or AC65, resulting in large potential drop. Moreover, it appears that E4 is active for the oxidation of borohydride since for potential greater than −0.6 V a significant positive current was observed that was absent in 6 M NaOH.

The comparison of Fig. 5a and b shows that the current density recorded at −0.6 V has decreased by a factor of six for AC65 while for MnO_2 a reduction in the current density by a factor of two only was observed. These results suggest that borohydride

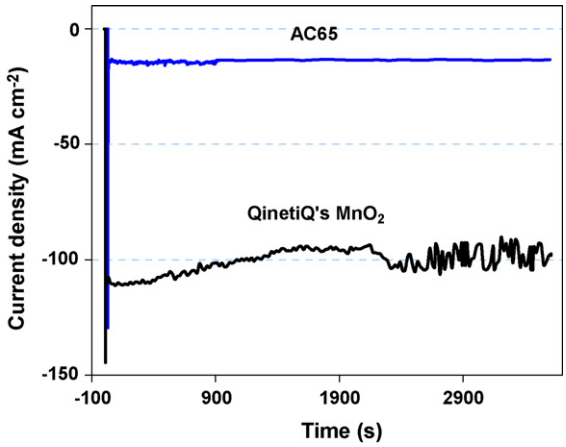

Fig. 6. Current response to polarisation of −0.5 V at different air-electrodes in 5% $NaBH_4$ in 6 M NaOH.

has a more detrimental effect on the performance of AC65 than MnO_2. Fig. 5b also shows that MnO_2 is inactive for the oxidation and chemical hydrolysis of BH_4^- ions and is consistent with the data reported in [16]. These results were further substantiated by the potential step experiments illustrated in Fig. 6 where the two electrodes were polarised at a potential of −0.5 V.

3.4. Fuel cell testing

QinetiQ's tubular fuel cells were assembled using membrane electrode assembly (MEA) comprising of nano-particulate gold as the anode, the anionic membrane and silver-based catalyst AC65 as the cathode. The latter functioned as air-breathing without any auxiliary facilities. In order to gain an insight of different phenomena arising at different electrode interfaces, a reference electrode was inserted in the tubular cell. The cell was polarised from open circuit voltage to 0.1 V in steps of 50 mV. The data is summarised in Fig. 7. Also included in this figure is the data obtained on commercial Au/C anode from E-Tek. Surprisingly, the current density measured on both systems was found to be fairly similar with a maximum power density of 12 mW cm^{-2}. It has to be pointed out that gold loading on the nano-particulate gold (0.8 mg cm^{-2}) was less than 1.8 mg cm^{-2} used in the commercial Au/C E-Tek electrode.

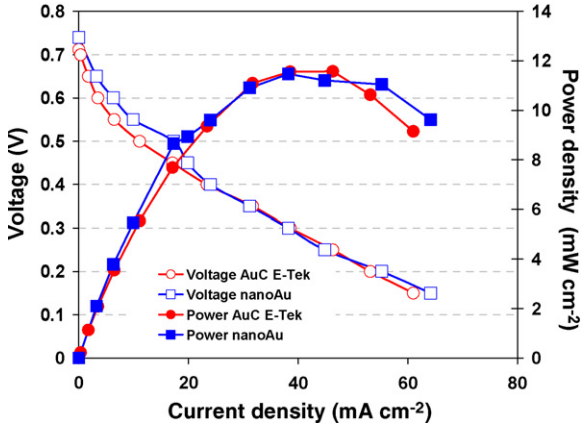

Fig. 7. Voltage and power density of fuel cells: AuC/AM/AC65 and nano-Au/AM/AC65.

Table 3
Nano-particulate Au anode/AM/AC65 cathode cell characteristics at 0.65 and 0.20 V

Cell current (mA)	Cell voltage (V)	Cathode voltage (V)	Anode voltage (V)
−30	0.65	−0.314	−0.963
−718	0.20	−0.626	−0.824

We have also summarised in Tables 3 and 4 the cell voltage, the voltage of cathode and the voltage of anode when the cell was polarised at different voltages. One possible reason that could explain the similar current obtained in both systems is the limitation of the cathode. Analysis of Tables 3 and 4 reveals that the nano-particulate gold is less polarised than the commercial Au/C electrode. The voltage swung from −0.963 to −0.824 V for the nano-particulate anode compared to a voltage swing of −0.840 to −0.542 V for the commercial Au/C electrode. However, in contrast to cells using the commercial Au/C as the anode, the cathode in the cell using nano-particulate gold was more polarised with a voltage swing of −0.314 to −0.626 V compared to −0.192 to −0.349 V for cell with Au/C E-Tek anode. This discrepancy could be due to a batch-to-batch variation in the distribution of the catalyst in the commercial air-electrode.

These results agree well with the data obtained by voltammetry and potential steps on AC65 electrode the performances of which were more deteriorated in presence of BH_4^-. The substitution of AC65 by MnO_2 while maintaining the other components of the fuel cell the same, i.e. the anionic membrane and the nano-particulate gold, should result in better performances. To verify this hypothesis, a tubular cell was built and tested. The results are shown in Fig. 8. For comparison we have also added the data on the cell that used AC65 as the cathode. The maximum power density was increased by a factor of 2.3. The maximum power density was 28 mW cm^{-2} for the cell using MnO_2 as the cathode compared to 12 mW cm^{-2} for the cell using AC65 as the cathode. The improved performances obtained in this case can only be attributed to MnO_2 electrode. In fact, we have plotted in Fig. 8 the cell voltage, the voltage of the anode and the voltage of the cathode of the cell when the cell was polarised at different voltages. For comparison, we have also added the data of a fuel cell that used AC as the cathode.

Examination of Fig. 8 shows for the cell that used AC65 as the anode, the polarisation losses at AC65 is greater than MnO_2 while the polarisation on the anode for both cells is fairly similar. Thus, AC65 cathode was the limiting electrode, which is consistent with the data obtained on AC65 in 5 wt% $NaBH_4$ in 6 M NaOH by cyclic voltammetry and potential steps.

Table 4
Au/C E-Tek anode/AM/AC65 cathode cell characteristics at 0.65 and 0.20 V

Cell current (mA)	Cell voltage (V)	Cathode voltage (V)	Anode voltage (V)
−23	0.65	−0.192	−0.840
−691	0.20	−0.347	−0.542

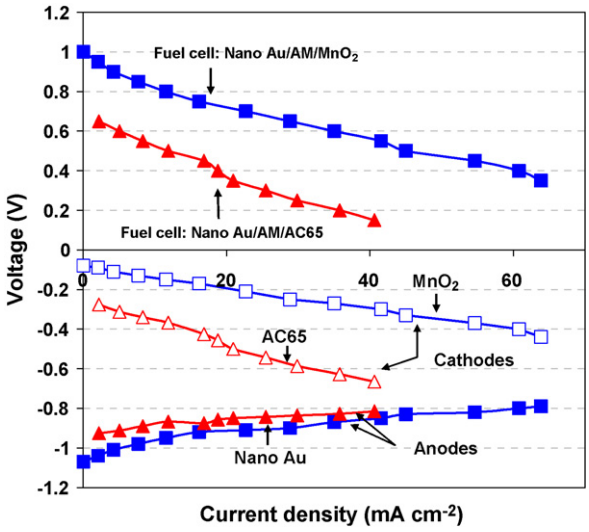

Fig. 8. Cell voltage and polarisation of cathodes and anodes vs. Hg/HgO in a two different fuel cells: 1) nano-Au/ AM /AC65; 2) nano-Au/AM/QinetiQ's MnO_2.

A fuel cell incorporating the nano-particulate bimetallic Au–Pt material, anionic membrane and composite MnO_2 was also assembled and evaluated. The OCV of this system was 1.09 V fairly similar to the fuel cell that used the nano-particulate gold as the anode. For current density lower than 30 mA cm^{-2}, the two fuel cells performed in a similar manner (see Fig. 9). However for current density higher than 30 mA cm^{-2}, the fuel cell using the nano-particulate gold anode showed higher power capability. The maximum power density of 20 mW cm^{-2} was measured compared to 28 mW cm^{-2} for the fuel cell system using the nano-particulate gold anode. The lower power capability found in the former case could arise from several factors, for instance loss of catalyst from the anode, limited access of fuel to the active sites and reduced conductivity of the membrane due to dehydration. To check the latter hypothesis, we flushed thoroughly the fuel cell first with distilled water for around 20 min and left it soaked overnight in distilled water in an attempt to re-hydrate the anionic membrane. Before embarking on the testing of the fuel cell, AC impedance was measured to measure the

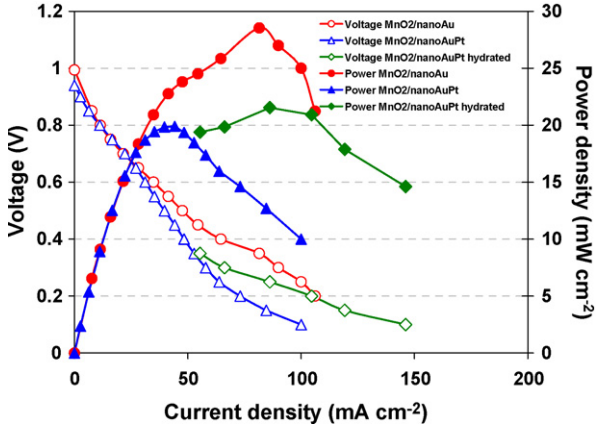

Fig. 9. Voltage and power density of fuel cells: nano-Au/MnO_2, nano-Au-Pt/MnO_2 and nano-Au-Pt/MnO_2 after hydration.

resistance of the membrane. Indeed, the resistance associated to the conductivity of the membrane was reduced by a factor of 10. After re-hydration of the membrane, the current density increases by a factor of two but the power density remains inferior to the fuel cell using the nano-particulate gold anode. It is possible that hydrolysis of borohydride occurring on the platinum sites generates hydrogen gas that will probably hinder the access of fuel to the active sites. It is also possible that loss of active materials from the current collector caused by the generation of hydrogen gas will lead to a reduced number of active sites.

4. Conclusion

Nano-particulate gold-based materials as well as commercial gold supported over carbon were investigated as possible alternative electrocatalysts for the oxidation of borohydride in alkaline medium. Cyclic voltammetry experiments conducted on these materials show very high activity for the nano-particulate materials compared to the commercial E-Tek Au/C-based materials despite a lower loading of gold ($0.8\,mg\,cm^{-2}$ compared to $1.0\,mg\,cm^{-2}$) and a lower interfacial area in the nano-particulate electrodes.

Two commercially available electrodes E4 which is a manganese-based electrode from Electric Fuel Ltd. and AC65 (Israel) a silver-based electrode, from Alupower/Yardney (USA) and a home-made composite electrode based on MnO_2 were investigated as electrocatalysts for oxygen reduction in presence and absence of 5 wt% of $NaBH_4$ in oxygenated 6 M NaOH.

The open circuit potential OCV of E4 electrode drops to around -0.6 V after 1 h immersion in oxygenated 5 wt% $NaBH_4$ in 6 M NaOH which makes it unsuitable to be used as cathode material while MnO_2 composite electrode and AC65 give respectively a stable open circuit potential of -0.116 and -0.190 V after an hour immersion in the same solution. Cyclic voltammetry carried out on these electrodes in 5 wt% of $NaBH_4$ in oxygenated 6 M NaOH showed that BH_4^- had a detrimental effect on the performance of AC65 while MnO_2 maintained reasonable activity and stability for oxygen reduction.

The implementation of the nano-particulate gold-based materials and the air-electrodes along with a low-cost anionic membrane in QinetiQ's tubular cell design has led to power density exceeding $28\,mW\,cm^{-2}$ obtained at ambient temperature.

Acknowledgement

This work was carried out as part of the Weapons and Platform Effectors Domain of the MoD Research Programme.

References

[1] S. Gottesfeld, J. Pafford, J. Electrochem. Soc. 135 (1988) 2651.
[2] H. Igarashi, T. Fujino, M. Watanabe, J. Electroanal. Chem. 391 (1995) 119.
[3] A.K. Shukla, C.L. Jackson, K. Scott, Bull. Mater. Sci. 26 (2003) 207.
[4] C. Pone de Leo'n, F.C. Walsh, D. Pletcher, D.J. Browning, J.B. Lakeman, J. Power Sources 155 (2006) 172.
[5] C. Lamy, A. Lima, V. LeRuhn, F. Delime, C. Coutanceau, J.M. Leger, J. Power Sources 105 (2002) 181.
[6] J. Han, E.-S. Park, J. Power Sources 112 (2002) 477.
[7] A.S. Arico, S. Srinivasan, V. Antonucci, Fuel Cells 1 (2001) 1.
[8] A.K. Shukla, C.L. Jackson, K. Scott, R.K. Raman, Electrochim. Acta 47 (2002) 3401.
[9] S.C. Amendola, P. Onnerud, P.T. Kelly, P.J. Petillo, S.L. Sharp-Goldman, M. Binder, J. Power Sources 84 (1999) 130.
[10] Z.P. Li, B.H. Liu, K. Arai, S. Suda, J. Electrochem. Soc. 150 (2003) A868.
[11] E. Gyenge, Electrochim. Acta 49 (2004) 965.
[12] M. Chatenet, F. Micoud, I. Roche, E. Chainet, Electrochim. Acta 51 (2006) 5459.
[13] Y.-G. Wang, Y.-Y. Xia, Electrochem. Commun. 8 (2006) 1775.
[14] Y. Okinaka, J. Electrochem. Soc. 120 (1973) 739.
[15] B.H. Liu, S. Suda, J. Power Sources 164 (2007) 100.
[16] R.X. Feng, H. Dong, Y.D. Wang, X.P. Ai, Y.L. Cao, H.X. Yang, Electrochem. Commun. 7 (2005) 138.